Published in final edited form as:
Curr Biol. 2009 February 10; 19(3): 260–265. doi:10.1016/j.cub.2008.12.045.

Myosin II mediates local cortical tension to guide endothelial cell branching morphogenesis and migration in 3D

Robert S. Fischer[1], **Margaret Gardel**[2], **Xuefei Ma**[3], **Robert Adelstein**[3], and **Clare M. Waterman**[1]

[1] Laboratory of Cell and Tissue Morphodynamics, Cell Biology and Physiology Center, National Heart, Lung, and Blood Institute, National Institutes of Health, Bethesda, MD, 20892

[2] Department of Physics, University of Chicago, Chicago, IL, 60637

[3] Laboratory of Molecular Cardiology, Genetics and Developmental Biology Center, National Heart, Lung, and Blood Institute, National Institutes of Health, Bethesda, MD, 20892

Summary

A key feature of angiogenesis is directional control of endothelial cell (EC) morphogenesis and movement [1]. During angiogenic sprouting, endothelial “tip cells” directionally branch from existing vessels in response to biochemical cues such as VEGF or hypoxia, and migrate and invade the surrounding extracellular matrix (ECM) in a process that requires ECM remodeling by matrix metalloproteases (MMPs) [2–4]. Tip EC branching is mediated by directional protrusion of subcellular pseudopodial branches [5,6]. Here we sought to understand how EC pseudopodial branching is locally regulated to directionally guide angiogenesis. We develop an *in vitro* 3D EC model system where migrating ECs display branched pseudopodia morphodynamics similar to those in living zebrafish. Using this system, we find that ECM stiffness and ROCK-mediated myosin II activity inhibit EC pseudopodial branch initiation. Myosin II is dynamically localized to the EC cortex, and is partially released under conditions that promote branching. Local depletion of cortical myosin II precedes branch initiation, and initiation can be induced by local inhibition of myosin II activity. Thus, local downregulation of myosin II cortical contraction allows pseudopodium initiation to mediate EC branching and hence guide directional migration and angiogenesis.

In vivo, tip EC branching morphogenesis occurs in a compliant three-dimensional (3D) environment. Branching is regulated in part by actomyosin-mediated cellular sensing of environmental compliance and dimensionality. In “compliance mechanosensing,” ECM stiffness and myosin II-mediated cell contractility are engaged in a feedback loop [7]. Stiffness is sensed by cell-ECM adhesions, which mediate RhoA activation of Rho-kinase (ROCK) to enhance adhesion and myosin II-mediated contractility [8,9]. “Dimensionality mechanosensing” promotes differential responses to 2-D and 3-D ECM environments [10, 11]. For example, engagement of integrins on both dorsal and ventral surfaces of cells in 2D culture alters cytoskeletal organization, cell morphology and migration compared to response to engagement of the same receptors only on the ventral surface [12,13]. The notion that both cytomechanical and intracellular signaling is critical for angiogenesis is well established [14,

Supplemental Data

Supplemental data, include six figures, fourteen movies, and a table of statistical comparisons, as well as further experimental details can be found online.

15]. Since directed tip EC migration requires ECM degradation by MMPs, local ECM loosening and remodeling near sites of adhesion may be critical to directing EC migration *in vivo* [3]. However, how cues of compliance and dimensionality feed back to regulate the actomyosin machinery to mediate EC branching morphogenesis and tip EC migration in physiological environments is unknown.

Results and Discussion

To facilitate our studies of tip EC migration in 3D, we first characterized dynamics of tip ECs *in vivo* to serve as a basis for development of a physiologically relevant model (Fig 1A–C, and [6]). We employed 4D microscopy to analyze the ECs in developing intersegmental vascular arches of zebrafish embryos stably expressing GFP driven by the endothelial-specific *fli-1* promoter (Fig 1A–C). Similar to previous reports [5], tip ECs explored using long, thin protrusions that extended and retracted with characteristic rates (see Movies 1 and 4). EC protrusions displayed branches, small lamellipodia-like structures and bulges along their lengths and at their tips (see Fig 1B, 1C). Because these protrusions are not yet characterized according to their content of F-actin regulatory components, we will refer to them generically as “pseudopodia”.

For our *in vitro* EC model, we used mouse aortic explants embedded within a 3D collagen fibrillar matrix. ECs migrated from explants singly as well as collectively in multicellular tube structures (Fig 1D, E, F, G), in both cases retaining endothelial differentiation status (Supp. Fig 1). Both single ECs and ECs at the tips of multicellular tubes form branched pseudopodia similar (Fig 1E, F) in morphology to pseudopodia on tip ECs *in vivo* (Fig 1B, C). Time-lapse imaging revealed that both single and tip mouse ECs on multicellular tubes approximated zebrafish tip EC dynamics *in vivo*, moving through the collagen matrix using similar branched pseudopodia with small lamellipodia on their sides and ends (Fig 1G, Movies 3 and 4, Supp. Fig 2A, B). Importantly, the protrusion and retraction rates (Fig 1G, H), length range (~10–78 μm *in vivo*, ~10–95 μm *in vitro*), and temporal persistence (11.3 +7.8 min *in vitro*; 14.0 + 4.3 min *in vivo*) of pseudopodia on both single and tip mouse ECs in collagen gels were similar to those of pseudopodia on zebrafish tip ECs (Movie 4). Thus, although the overall movement of single and tip ECs differs because of cell-cell-junctions, single mouse EC pseudopodial protrusion behavior is similar to that of tip ECs *in vitro* and *in vivo* [16].

For some experiments, we desired to control the compliance of the *in vitro* 3D environment. To affect compliance without altering 3D collagen access, we covalently coupled 3D collagen matrices to polyacrylamide (PA) gels of defined elastic modulus (Fig 2) and affixed these to microscope coverslips, to make collagen/PA/glass “sandwich gels”. ECs in the collagen at the PA-collagen interface (Fig 2A) engage on their ventral surfaces collagen covalently coupled to PA of defined stiffness, but also engage dorsal collagen in the 3D matrix. Since the collagen matrices were softer than the underlying PA (see Supplemental Methods), the maximum stiffness encountered by the cells was collagen coupled to the PA. In 0.45 kPa collagen/PA/glass sandwich gels, ECs displayed an elongated, spindle-like morphology with extended pseudopodial branches. Quantification of their pseudopodial protrusion and retraction behavior revealed dynamics similar to tip ECs in zebrafish *in vivo* and mouse ECs in 3D collagen matrices (Figs 1E, F, 2B, also compare Supp. Movies 3 and 6, right). In conclusion, single mouse ECs in both collagen matrices and collagen/PA/glass sandwich gels provide a physiologically relevant 3D model system amenable to high resolution microscopy to study EC protrusion and branching.

Pseudopodial branching is initiated by lamellipodial protrusion and inhibited by ECM stiffness and ROCK-mediated myosin II activity

We first characterized pseudopodial branch initiation and its contribution to directional migration. During migration, which was generally radially away from the aortic explant, Ecs exhibited localized sites of lamellipodial activity along their branches and cell bodies. Some lamellipodia extended away from the EC to form new pseudopodial branches (Supp. Fig 2A, Movies 3 and 5). Most pseudopodia rapidly retracted back into the cell body, but a few persisted. The persistent branchs that generated sufficient adhesion and force on the ECM (indicated by collagen deformation, Supp. Fig 2B and Supp. Movie 5) to pull the cell body consequently changed the direction of cell migration. Thus, EC branches are initiated from lamellipodia, and persistent branches mediate EC pathfinding.

To determine the role of ECM compliance in regulating branching, we examined ECs in collagen/PA/glass sandwich gels. ECs in soft sandwich gels (0.45kPa PA) branched and migrated similarly to ECs in 3D collagen matrices (Fig 2B, and Movies 6 right and 7, top). Stiffening the PA in the sandwich gel (14kPa) induced spindle-shaped ECs with significantly fewer branches (Fig 2D), but did not alter overall radial migration from the explant (Fig 2E, Movies 6 left, and 7 bottom). Limiting collagen access to 2D by replating ECs on top of a 2D layer of collagen covalently coupled to soft PA (0.45kPa) induced cell aggregation, with some single cells exhibiting small lamellae and a few branched extensions (Fig 2H, Supp. Movie 8). Stiffening the PA in this 2D system (14kPa) caused ECs to spread with large, unbranched lamellae, similar to ECs cultured on plastic or glass (Fig 2I; see also Supp. Movie 8). Quantification of EC branch number showed that, for the same compliance, 3D collagen engagement enhanced cell branching compared to 2D (Fig 2G). Therefore, increased ECM stiffness inhibits EC branching morphogenesis, and three dimensionality is synergistic with compliance in promoting branching.

To determine if inhibition of EC branching of ECs by 3D ECM stiffness is linked to myosin II activity, we pertrubed EC myosin II function in either stiff (14kPa) or soft (0.45 kPa) collagen/PA/glass sandwich gels and examined branch formation. Myosin II ATPase inhibition with 30 μM blebbistatin significantly increased EC branching in both soft (Fig 2C) and stiff (Fig 2F) sandwich gels. The response of ECs to both decreased ECM stiffness and inhibition of myosin II was synergistic as compared with either treatment alone (Fig 2D), suggesting that softer ECM may enhance EC sensitivity to decreased myosin II activity.

Myosin II can be regulated by phosphorylation of its light chains by myosin light chain kinase (MLCK) or ROCK [17,18]. To determine which pathway mediated myosin II regulation of EC branching, we used pharmacological inhibitors on ECs in 3D collagen matrices. As observed in collagen/PA/glass sandwich gels, inhibition of myosin II ATPase with blebbistatin in 3D collagen increased EC branching as compared to controls (Supp. Fig 3;Movie 9), while the inactive +/+ enantiomer of blebbistatin had no effect (Supp. Fig 3). Inhibition of Rho GTPase by cell permeable C3-exoenzyme or ROCK by either 10μM Y-27632, or 2 μM H-1152 (Supp. Fig 3) [19] also increased EC branching. ROCK-inhibited cells maintained bipolar morphology (Supp. Fig 3) and continued to move, but were unable to define a leading versus trailing end (Supp. Movie 9). Inhibition of MLCK with 1–2 μM ML-7 did not enhance EC branching, but promoted blebbing (Supp. Fig 3).

Pseudopodium initiation, protrusion and retraction may all contribute to EC steady-state branch morphology. To identify which of these processes are regulated by myosin II, we perturbed myosin II function in ECs in collagen matrices and quantified parameters of pseudopodial branch dynamics (Fig 3A–C). Compared to controls, either blebbistatin or Y-27632 had no significant effect on protrusion rates, but decreased pseudopodia retraction rates, (Fig 3A, B).

Y-27632 also increased the frequency of pseudopodium initiation (defined as extensions ≥ 5μm from the cell body) (Fig 3C). Similarly, comparing pseudopodium initiation was increased in ECs in soft compared to stiff collagen/PA/glass sandwich gels (Fig 3C). The complex shape of blebbistatin-treated ECs precluded reliable quantification of branch initiation. However, together these data show that contractility via Rho/ROCK-mediated myosin II activity and/or ECM stiffness inhibits EC branching by both blocking pseudopodium initiation and retracting branches after their successful initiation.

Regulation of branch initiation via myosin II controls directed EC migration and ECM invasion

Given that ECs follow the direction of the most stable branch, increased branching could affect EC invasion into 3D ECM and/or migration directional persistence. In control collagen matrices, ECs invaded extensively into the ECM (Fig 3G, and Movie 9), while inhibition of myosin II (Fig 3G) or ROCK (not shown) markedly reduced this invasion distance. Quantification showed that reduced invasion was due to decreases in both EC speed and directional persistence (Fig 3E, F). With blebbistatin, directional persistence and speed were affected by both a lack of EC polarization due to superfluous pseudopodia as well as decreased tail retraction, while ROCK inhibition had a stronger effect on polarization than speed (Movie 9). (Fig 3D). This contrasts cells in 2D culture, where myosin II perturbation decreases directional persistence, but enhances cell speed [22]. Additionally, ECs in soft (0.45 kPa) collagen/PA/glass sandwich gels showed decreased directional persistence relative to those in stiffer (14 kPa) sandwich gels (Fig 3D, E). Thus, Rho/ROCK-mediated myosin II contractility or ECM stiffness promotes 3D ECM invasion by inhibiting EC branching to encourage directional persistence and enhance migration speed.

Myosin II activity and stability within the F-actin cortex regulates EC branching

To understand how myosin II inhibits pseudopodial branch formation, we examined the 3D localization of myosin IIs in ECs in 3D collagen matrices from transgenic mice in which endogenous myosin IIB was replaced by GFP-myosin IIB. F-actin, GFP-myosin IIB and myosin IIA (by immunofluorescence) all co-localized to the cortex, while both myosin II isoforms additionally formed a fibrillar cytoplasmic pool (Fig 4A–C and Supp. Fig 4A–D). Glancing optical sections of the cortex showed that myosin IIB and F-actin formed longitudinal bundles reminiscent of actomyosin bundles or stress fibers in 2D cultures [23] (Fig 4 and Movies 10 and 11). ROCK-mediated myosin II contractility was required for forming/maintaining the bundles, since Y-27632 or blebbistatin abolished them (Fig 4E–G,Supp. Movie 12, and Supp. Fig 4E–H). Time-lapse imaging showed that myosin IIB puncta formed and then coalesced into a web-like array behind the advancing tip of newly protruding pseudopodia (Movie 11,Fig 4D, H), similar to punctae in the lamella of cells in 2D culture [24]. (Movie 11). Thus, myosin II acts at the cell cortex, where it is dynamically co-localized with F-actin.

To determine if myosin II activity is regulated under conditions that modulate EC branching, we quantified Ser19 phosphomyosin II light chain by immunofluorescence of ECs in either soft (300 Pa) or stiff (14.5 kPa) collagen/PA/glass sandwich gels (Fig 4I). Ratio imaging with F-actin staining revealed a higher phosphomyosin II light chain:F-actin level in stiffer as compared to softer ECMs (Supp. Fig 6A). In addition to regulation by light chain phosphorylation, myosin II activity could be modulated by the stability of its cortical binding. To test this, we analyzed fluorescence recovery after photobleaching (FRAP) of GFP-myosin IIB at the EC cortex in soft (300 Pa) versus stiff (14.5 kPa) collagen/PA/glass sandwich gels (Fig 4J,K, Supp. Fig 6B). This revealed that in stiffer sandwich gels, a significantly larger

fraction of GFP-myosin IIB was stably associated with the cortex as compared to ECs in softer environments (Fig 4J). Although fluorescence recovery of the mobile fraction of cortical GFP-myosin IIB was faster in stiff compared to soft ECMs, the difference was not significant (Fig 4K), suggesting that the mobile fraction likely recovers via the same mechanism in the two conditions. In both soft and stiff ECMs, cytosolic GFP-myosin IIB fluorescence recovered rapidly and completely (data not shown). Thus, ECM stiffness may inhibit pseudopodial branching by both promoting myosin II's light chain phosphorylation and stable association with the EC cortex.

We next hypothesized that local down-regulation of cortical myosin II may allow pseudopodial branch initiation. In support of this, time-lapse images of GFP-myosin IIB showed that local alterations in cortical GFP-myosin IIB density preceded pseudopodial initiation. Prior to branch initiation, myosin IIB localized relatively uniformly along the cortex. Local thinning of the myosin IIB fluorescence caused gaps in localization flanked by brighter puncta, followed by lamellipodial protrusions extending from the gaps, and these lamellipodia went on to form persistent pseudopodial branches. Thus, local depletion of cortical myosin IIB precedes lamellipodium-mediated branch initiation.

To determine of local inhibition of cortical myosin II is sufficient to induce pseudopodial branch formation, we applied blebbistatin locally to unbranched regions of ECs in 3D collagen matrices using a microinjection pipette. Remarkably, this caused lamellipodial protrusion and pseudopodium extension near the point of application and towards the pipette tip in 9/20 samples (Fig 4M; Movie 14). Branches were never induced on the cell side opposite the local application, nor with vehicle alone (0/20 samples, $P= 3.3 \times 10^{-4}$; F/Fcrit= 3.79). Thus, local inhibition of cortical myosin II function can induce EC branching.

We propose a model of myosin II regulation of directed EC migration in a heterogenous, physiological 3D ECM environment (Supp. Fig 7). *In vivo,* local cues such as VEGF or hypoxia are likely transduced by tip ECs into signals that induce transient lamellipodial protrusions. Myosin II generates tension in the EC cortex to retract most protrusions. In regions where local ECM loosening (e.g, by MMP action) is encountered, contractility is locally downregulated by mechanosensory feedback that reduces light chain phosphorylation and releases cortical myosin II. Local myosin II downregulation allows lamellipodia to initiate a branch by "escaping" retraction by cortical tension. For the branch to change EC migration direction, the exploratory lamellipodium at its tip it must encounter and adhere to more distal ECM stiff enough to allow reestablishment of actomyosin contractility to pull the cell in the new direction. Thus, in uniformly soft ECMs, ECs initiate many branches, and fewer branches are successful in stably changing direction, decreasing migration polarity and directional persistence. Conversely, in stiffer ECM, fewer pseudopodia branches escape myosin II cortical tension, thereby focusing migration along collagen fibrils in the existing branch direction. Our data provide a mechanistic framework to understand long-held ideas regarding the role of the Rho pathway, myosin II contractility and ECM mechanics in vascular development in normal and tumor tissue, and endothelial cell migration both *in vivo* and *in vitro* [14] [27] [28], via regulation of myosin II activity and dynamics at the cell cortex.

Methods

Methods have been described in general in the text. For experimental details, please see Supplemental Materials.

Supplementary Material

Refer to Web version on PubMed Central for supplementary material.

Acknowledgments

We thank Roberta Nowak and Velia Fowler (Scripps Research Institute, La Jolla, CA) for maintaining GFP-actin mice, Konstantin Stoletov and Richard Klemke (UCSD, San Diego, CA) for *fli1-gfp* zebrafish embryos and Gaudenz Danuser (Scripps) for technical advice and constructive discussion.

References

1. Carmeliet P. Mechanisms of angiogenesis and arteriogenesis. Nat Med 2000;6:389–395. [PubMed: 10742145]
2. Gerhardt H, Betsholtz C. How do endothelial cells orientate? EXS 2005:3–15. [PubMed: 15617467]
3. Heissig B, Hattori K, Friedrich M, Rafii S, Werb Z. Angiogenesis: vascular remodeling of the extracellular matrix involves metalloproteinases. Curr Opin Hematol 2003;10:136–141. [PubMed: 12579040]
4. Hotary KB, Yana I, Sabeh F, Li XY, Holmbeck K, Birkedal-Hansen H, Allen ED, Hiraoka N, Weiss SJ. Matrix metalloproteinases (MMPs) regulate fibrin-invasive activity via MT1-MMP-dependent and -independent processes. J Exp Med 2002;195:295–308. [PubMed: 11828004]
5. Lawson ND, Weinstein BM. In vivo imaging of embryonic vascular development using transgenic zebrafish. Dev Biol 2002;248:307–318. [PubMed: 12167406]
6. Gerhardt H, Golding M, Fruttiger M, Ruhrberg C, Lundkvist A, Abramsson A, Jeltsch M, Mitchell C, Alitalo K, Shima D, et al. VEGF guides angiogenic sprouting utilizing endothelial tip cell filopodia. J Cell Biol 2003;161:1163–1177. [PubMed: 12810700]
7. Peyton SR, Kim PD, Ghajar CM, Seliktar D, Putnam AJ. The effects of matrix stiffness and RhoA on the phenotypic plasticity of smooth muscle cells in a 3-D biosynthetic hydrogel system. Biomaterials 2008;29:2597–2607. [PubMed: 18342366]
8. Beningo KA, Hamao K, Dembo M, Wang YL, Hosoya H. Traction forces of fibroblasts are regulated by the Rho-dependent kinase but not by the myosin light chain kinase. Arch Biochem Biophys 2006;456:224–231. [PubMed: 17094935]
9. Olson MF. Contraction reaction: mechanical regulation of Rho GTPase. Trends Cell Biol 2004;14:111–114. [PubMed: 15055199]
10. Frey MT, Tsai IY, Russell TP, Hanks SK, Wang YL. Cellular responses to substrate topography: role of myosin II and focal adhesion kinase. Biophys J 2006;90:3774–3782. [PubMed: 16500965]
11. Discher DE, Janmey P, Wang YL. Tissue cells feel and respond to the stiffness of their substrate. Science 2005;310:1139–1143. [PubMed: 16293750]
12. Beningo KA, Dembo M, Wang YL. Responses of fibroblasts to anchorage of dorsal extracellular matrix receptors. Proc Natl Acad Sci U S A 2004;101:18024–18029. [PubMed: 15601776]
13. Even-Ram S, Yamada KM. Cell migration in 3D matrix. Curr Opin Cell Biol 2005;17:524–532. [PubMed: 16112853]
14. Mammoto A, Mammoto T, Ingber DE. Rho signaling and mechanical control of vascular development. Curr Opin Hematol 2008;15:228–234. [PubMed: 18391790]
15. Ingber DE. Mechanical signaling and the cellular response to extracellular matrix in angiogenesis and cardiovascular physiology. Circ Res 2002;91:877–887. [PubMed: 12433832]
16. Friedl P. Prespecification and plasticity: shifting mechanisms of cell migration. Curr Opin Cell Biol 2004;16:14–23. [PubMed: 15037300]
17. Conti MA, Adelstein RS. Nonmuscle myosin II moves in new directions. J Cell Sci 2008;121:11–18. [PubMed: 18096687]
18. Clark K, Langeslag M, Figdor CG, van Leeuwen FN. Myosin II and mechanotransduction: a balancing act. Trends Cell Biol 2007;17:178–186. [PubMed: 17320396]
19. Ikenoya M, Hidaka H, Hosoya T, Suzuki M, Yamamoto N, Sasaki Y. Inhibition of rho-kinase-induced myristoylated alanine-rich C kinase substrate (MARCKS) phosphorylation in human neuronal cells by H-1152, a novel and specific Rho-kinase inhibitor. J Neurochem 2002;81:9–16. [PubMed: 12067241]

20. Kubo T, Endo M, Hata K, Taniguchi J, Kitajo K, Tomura S, Yamaguchi A, Mueller BK, Yamashita T. Myosin IIA is required for neurite outgrowth inhibition produced by repulsive guidance molecule. J Neurochem 2008;105:113–126. [PubMed: 18005226]

21. Loudon RP, Silver LD, Yee HF Jr, Gallo G. RhoA-kinase and myosin II are required for the maintenance of growth cone polarity and guidance by nerve growth factor. J Neurobiol 2006;66:847–867. [PubMed: 16673385]

22. Lo CM, Buxton DB, Chua GC, Dembo M, Adelstein RS, Wang YL. Nonmuscle myosin IIb is involved in the guidance of fibroblast migration. Mol Biol Cell 2004;15:982–989. [PubMed: 14699073]

23. Kolega J. Asymmetry in the distribution of free versus cytoskeletal myosin II in locomoting microcapillary endothelial cells. Exp Cell Res 1997;231:66–82. [PubMed: 9056413]

24. Verkhovsky AB, Svitkina TM, Borisy GG. Myosin II filament assemblies in the active lamella of fibroblasts: their morphogenesis and role in the formation of actin filament bundles. J Cell Biol 1995;131:989–1002. [PubMed: 7490299]

25. Bentley K, Gerhardt H, Bates PA. Agent-based simulation of notch-mediated tip cell selection in angiogenic sprout initialisation. J Theor Biol 2008;250:25–36. [PubMed: 18028963]

26. Siekmann AF, Lawson ND. Notch signalling limits angiogenic cell behaviour in developing zebrafish arteries. Nature 2007;445:781–784. [PubMed: 17259972]

27. Mavria G, Vercoulen Y, Yeo M, Paterson H, Karasarides M, Marais R, Bird D, Marshall CJ. ERK-MAPK signaling opposes Rho-kinase to promote endothelial cell survival and sprouting during angiogenesis. Cancer Cell 2006;9:33–44. [PubMed: 16413470]

28. Matsumoto T, Yung YC, Fischbach C, Kong HJ, Nakaoka R, Mooney DJ. Mechanical strain regulates endothelial cell patterning in vitro. Tissue Eng 2007;13:207–217. [PubMed: 17518594]

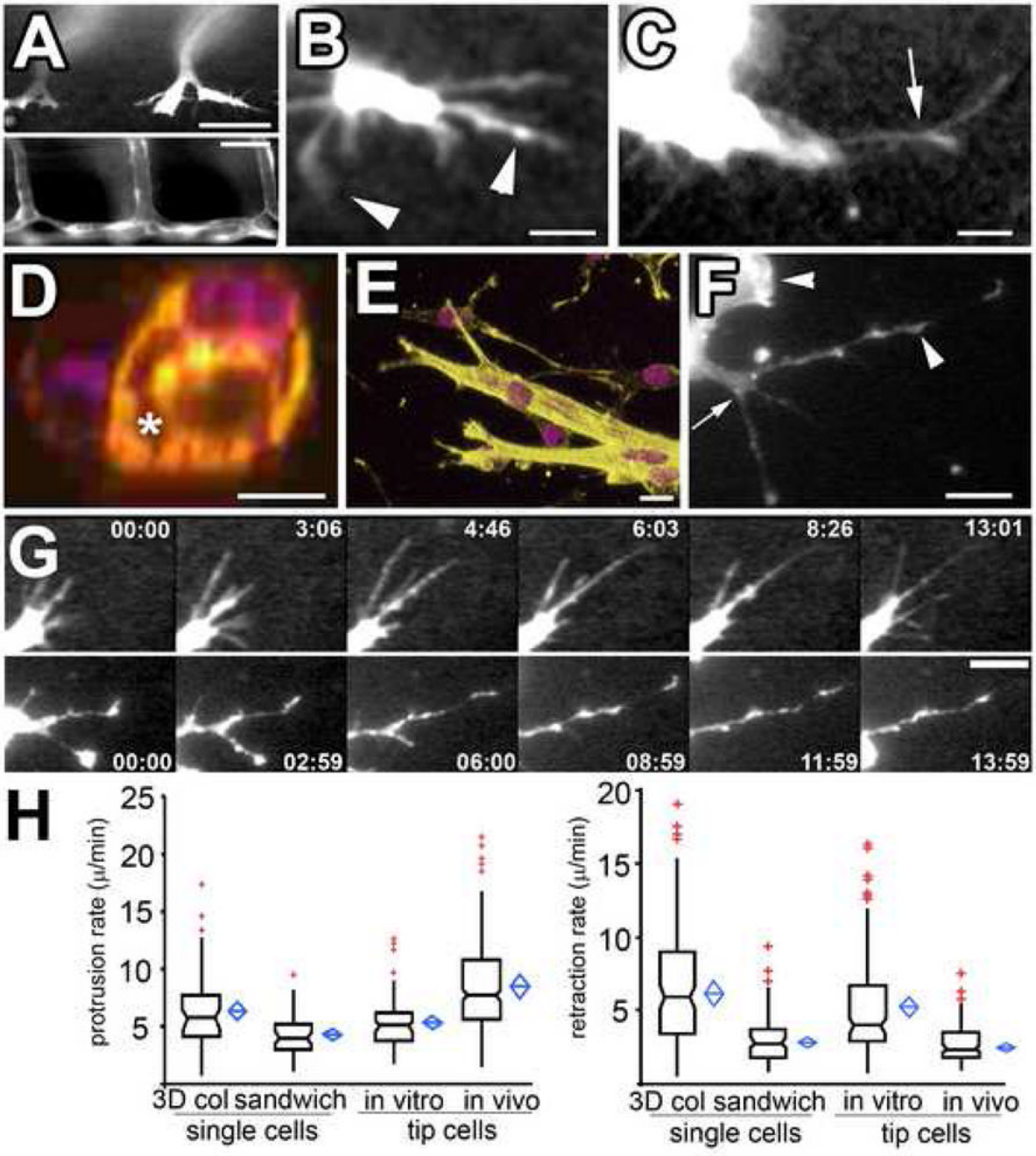

Figure 1. ECs *in vivo* and in 3D collagen matrices *in vitro* exhibit similar pseudopodial morphology and dynamics

(A–C) Confocal images of living ECs expressing GFP during zebrafish embryonic angiogenesis (see Supp. Movie 1). Intersegmental vessels (A, bottom), 7d post-fertilization, form from branched tip ECs (A, top, 24hr post-fertilization). (B,C) Higher magnification views of living tip ECs (Supp. Movies 1, 3). Arrows, branch points along pseudopodia; arrowheads, tip and side lamellipodia-like bulges. (D) Cross-section of mouse endothelial tube structure formed in 3D collagen matrices; violet, DAPI stained nuclei; yellow, phalloidin-stained F-actin; asterisk, lumen formed between cells. (E) 3D reconstructions of mouse endothelial tube tips formed in 3D collagen. (F) Confocal image of living mouse aortic ECs expressing GFP-

β-actin in a 3D collagen matrix. Branch points (arrow) and lamellipodia (arrowhead) and bulges along pseudopodia are highlighted. (G) Images from time-lapse confocal series showing protrusion dynamics of zebrafish tip ECs *in vivo* (top) and in mouse ECs in 3D collagen matrices *in vitro* (bottom); time in min:sec shown. (H) Protrusion (left graph) and retraction rates (right graph) of pseudopodia of single ECs or tube tip cells in 3D collagen matrices ("3D col"), 450 kPa collagen/PA/glass sandwich gels ("sandwich") and zebrafish tip ECs *in vivo.* In this and subsequent figures, boxes: median and center quartiles, blue diamonds: 95% confidence limit means, red plusses: outliers of >1.5 and <3.0 interquartile range. Bars equal (A), top 40μm, bottom 80 μm, (B, C): 21μm, (D): 10 μm, (E, G): 12 μm, (F): 31μm. For statistical analysis, see Supp. Table I.

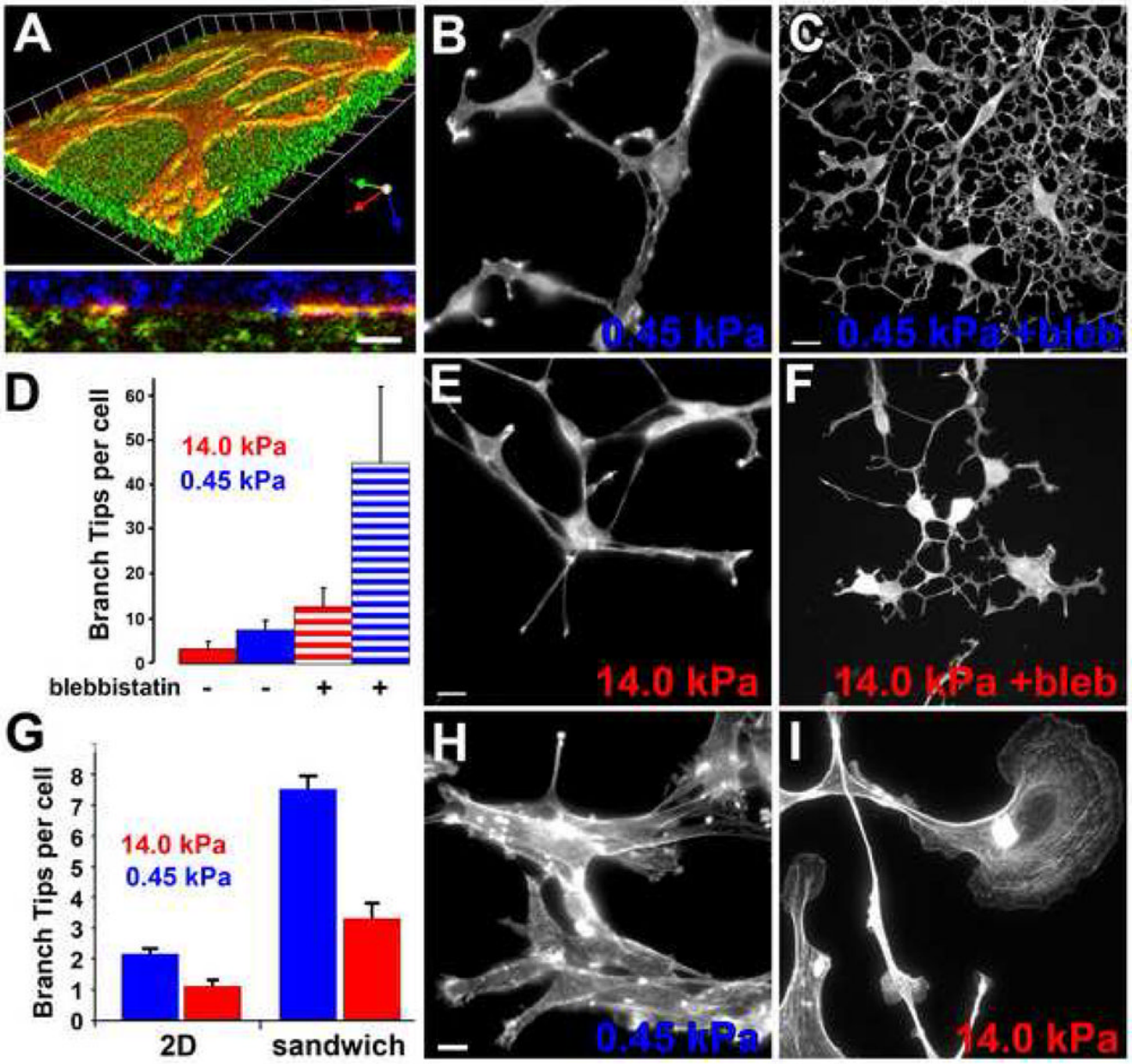

Figure 2. ECM stiffness is synergistic with ROCK-mediated myosin II activity in inhibiting EC branching

(A–E) Mouse aortic ECs grown in collagen/PA/glass "sandwich gels" (see text, Supp. Methods) with F-actin stained with BODIPY-phallacidin. (A) 3D reconstruction of confocal image z-series of mouse aortic cells expressing GFP-actin (red) in a collagen/PA/glass sandwich gel. Above: skewed view, grid unit= 9.8μm, below: X–Z view. Cell is at the interface between the collagen covalently bound to the PA (embedded with fluorescent microspheres, green) and surrounding 3D collagen (immunolabeled, blue). (B,C,E,F) Maximum intensity projections of confocal image z-series. ECs in soft (B,C; 0.45 kPa) or stiff (E; F 14 kPa) collagen/PA/glass sandwich gels, with (30μM; C, F) or without (B,E) blebbistatin treatment. (C) Quantification of branches per cell for ECs in collagen/PA/glass sandwich gels of the stiffness shown, with or without 30μM blebbistatin treatment. (H, I) Mouse ECs stained with

BODIPY-phallacidin on soft (G, 0.45 kPa) or stiff (H, 14 kPa) PA gels covalently coupled with a 2D layer of collagen.(G) Quantification of branch tips per cell on 2D collagen/PA substrates versus in collagen/PA/glass sandwich gels. Bars: (A, bottom, C, F, H, I), 12μmμm; (B,E), 9 μm. Error bars in (C) indicate SD, in (G) indicate SEM. For statistical analysis, see Supp. Table I.

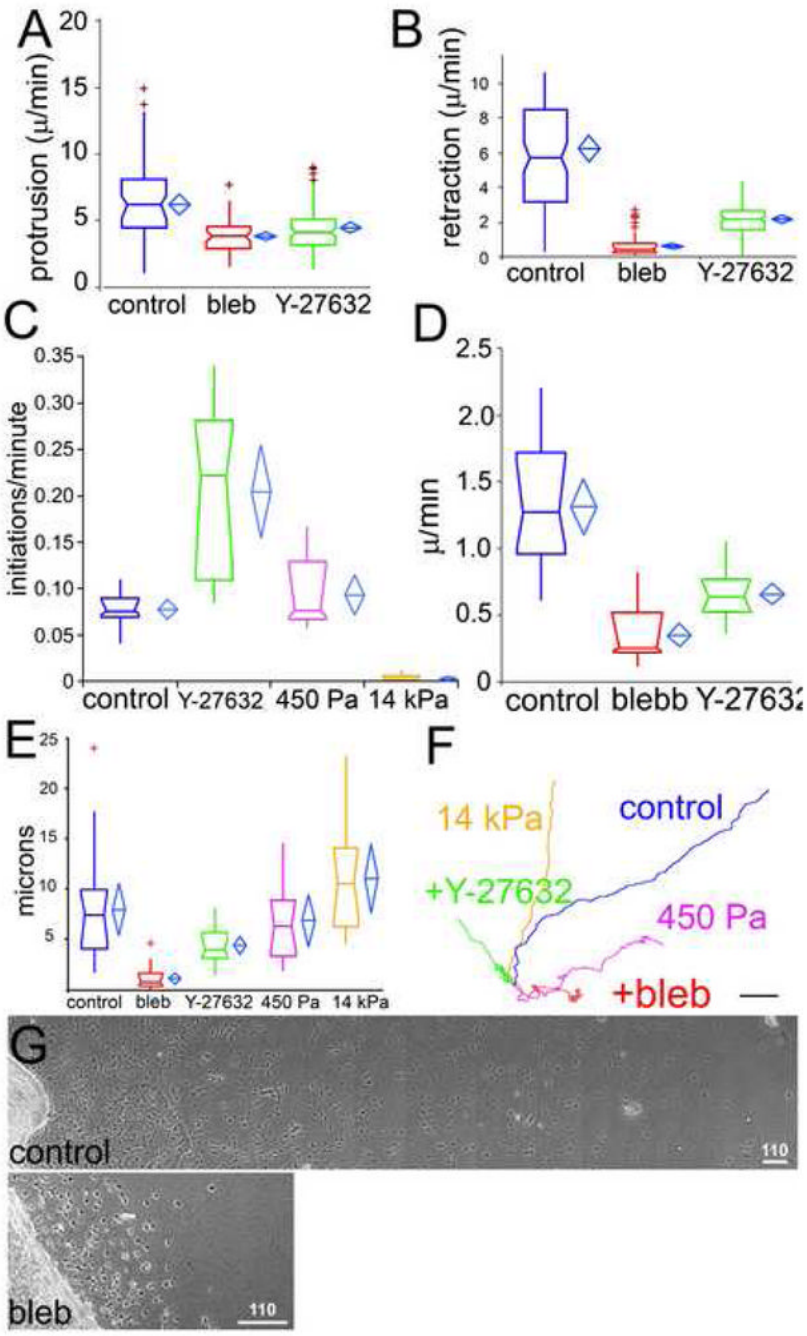

Figure 3. ROCK-mediated myosin II activity regulates pseudopodial dynamics and EC migration and invasion in 3D collagen gels

Parameters were measured from phase-contrast time-lapse movies of mouse aortic ECs in 3D collagen matrices (untreated (control) or treated with 30μM blebbistatin (bleb) or 10μM Y-27632) or in collagen/PA/glass sandwich gels of the indicated elastic moduli (450 Pa, 14kPa). Protrusion (A) and retraction (B) rates of individual pseudopodia. (C) Pseudopod initiation frequency per cell per minute (see Supp. Methods). EC migration speed (D) and migration directional persistence distance (E) measured as described [22]. (F) Example of 189 min long EC migration path traces. For statistical analysis, see Supp. Table I. (G) Montages

of images of mouse aortic cultures in 3D collagen matrices after 2d treatment with either vehicle (control) or 30uM blebbistatin (bleb). Bars in F=10μm, G=110μm.

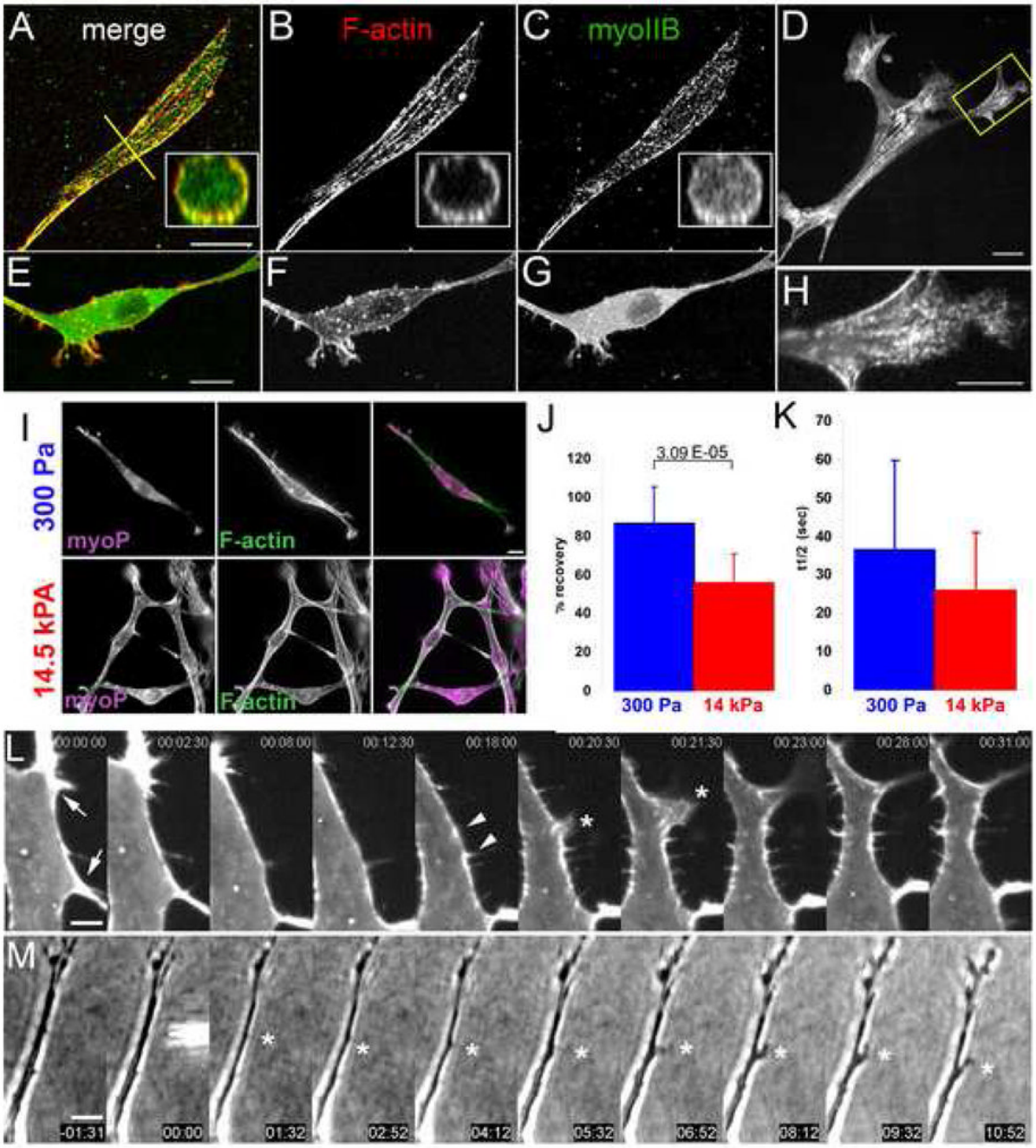

Figure 4. Myosin II activity and stability within the F-actin cortex regulates EC branching

(A–D) Maximal projections of 3D reconstructions of laser-scanning confocal z-image series of GFP myosin IIB (C,G), and bodipy phallacidin staining of F-actin (B,F) in mouse ECs in 3D collagen matrices. Insets, X–Z cross-sections taken along the yellow lines in (A). (E–G) Similar EC to in (A–C) but treated with 10uM Y27632. (D, H) Single spinning-disk confocal image of a living mouse EC expressing GFP-myosin IIB (H) Magnification of the area boxed in (D). Bars, 14μm (A–C) 10μm (E–G), 4μm (D,H). (I) Localization of serine-19 phosphorylated myosin light chain 2 ((myoP) by immunostaining) and F-actin (by fluorescent phalloidin) in mouse ECs in soft (300 Pa, top row) versus stiff (14.5kPa, bottom row) collagen/PA/glass sandwich gels. (J, K) Analysis of cortical GFP-myosin IIB FRAP in mouse aortic

ECs in collagen/PA/glass sandwich gels of the noted elastic moduli. (J) Mean percent fluorescence recovery to steady state. (K) Mean half-time of fluorescence recovery. (L) Montage of time-lapse confocal images of GFP-myosin IIB during pseudopodial branch initiation in mouse aortic ECs in 3D collagen gels; time in min:s,. Cortical GFP-myosin IIB intensity locally depletes (between arrows, times 00:00–12:30), collecting in two puncta (arrowheads). Asterisk, lamellipodial protrusion between former puncta, which extends into a pseudopodial branch (times 23:00–31:00). (M) Time-lapse phase-contrast images of local application of 40 μM blebbistatin to an EC in a collagen matrix. Time shown relative to drug application in min:s, microneedle containing drug visible at time 00:00. Asterisk marks application site. Bars: (A) 12μm, (D) 3.3μm, (E) 10 μm. Error bars in (B,C) indicate SD. For statistical analysis, see Supp. Table I.